2024 IEEE Conference on Computational Imaging Using Synthetic Apertures (CISA) | 979-8-3503-0864-8/24/$31.00 ©2024 IEEE | DOI: 10.1109/CISA60639.2024.10576358

DETECTION AND CHARACTERIZATION OF DRONES IN URBAN ENVIRONMENTS WITH SYNTHETIC APERTURE RADAR IMAGES

Maryam Abazarsa[1], Tzuyang Yu[1], Chiehping Lai[2], Jack Chuang[2], and David Griffith[2]

[1]Department of Civil and Environmental Engineering
University of Massachusetts Lowell
Lowell, MA 01854, USA
[2]National Institute of Standards and Technology (NIST),
Gaithersburg, MD 20899, USA

ABSTRACT

This work examines synthetic aperture radar (SAR) imaging of a commercial drone in an artificial urban environment. We used a 10 GHz frequency modulated continuous wave (FMCW) SAR imaging system with a 1.5 GHz bandwidth inside an electromagnetic anechoic chamber to generate SAR images for target detection and characterization. We considered combinations of two ranges, two cross-ranges, and five elevation angles. We constructed a brick wall inside the anechoic chamber and behind the drone to simulate the scenario of a drone flying very close to structures in an urban environment. From the initial SAR imaging and simulation results, we found that SAR imaging can detect and distinguish different drone orientations in an artificial urban environment.

***Index Terms*—** Drones, SAR imaging, urban environment, simulation

1. INTRODUCTION

Unmanned airborne vehicles (UAV) and systems (UAS), or drones, are widely used in various applications in urban environments, such as for structural inspection [1], traffic surveillance [2], law enforcement [3], and counterterrorism [4]. Drones can also be used for intelligence and law enforcement, i.e., to collect information or jam wireless communications. Detecting and characterizing drones in urban environments with different types of background clutter (e.g., buildings) is essential to monitoring drone activities effectively.

We constructed a 3-D radar-drone model using REMCOM's Wireless Insite software. The tool provides ray-tracing information between the drone and radar transceiver. It is used to provide a reference from the theoretical point of view and has deterministic information, which helps the development of the SAR imaging algorithm. The model setup was very close to the laboratory setup. The background clutter, such as brick walls, glass windows, and other materials, can be drawn or imported from the third-party CAD database.

2. RESEARCH APPROACH

2.1 LABORATORY SAR IMAGING FACILITY

We used a laboratory 10 GHz frequency modulated continuous wave (FMCW) SAR imaging radar system with a 1.5 GHz bandwidth inside an anechoic chamber to generate all SAR images of a commercial drone. The drone has a 350 mm diagonal length, a 196 mm height, and a 289.5 mm length/width. We considered two range setups (R = 0.4 m and 1 m) and two cross-range values (CR = 0.4 m and 2 m) in the laboratory SAR imaging process. We used five tilt angles of the drone to simulate different orientations of the drone (0°, 30°, 45°, 60°, and 90°). Fig. 1 illustrates two angular drone orientations in our lab.

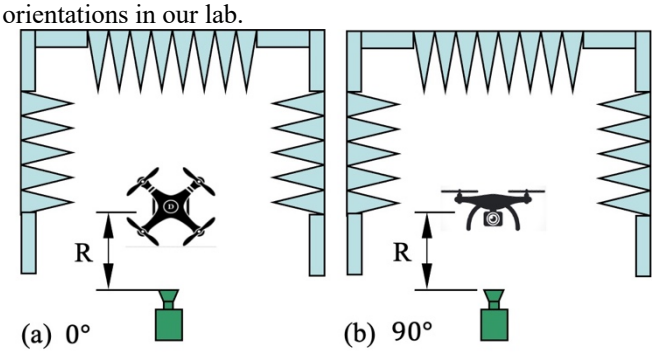

Fig. 1. Two angular drone orientations in the lab at UML.

2.2 SIMULATION MODEL

We used the software tool to create the SAR simulation model, shown in Fig. 2. The CAD model drone is the same size as the drone used in the measurements. The CAD drone has 25 000 faces. The SAR simulation model considers one range set (R = 0.4 m and CR = 2.0 m). There are 15 radar

Certain equipment, instruments, software, or materials are identified in this paper to specify the experimental procedure adequately. Such identification is not intended to imply recommendation or endorsement of any product or service by NIST, nor is it intended to imply that the materials or equipment identified are necessarily the best available for the purpose.

Authorized licensed use limited to: NIST Virtual Library (NVL). Downloaded on July 09,2025 at 17:37:20 UTC from IEEE Xplore. Restrictions apply.

locations, and the separation is around 15 cm (one half-wavelength). The background clutter can be imported into the model. We can simulate the five tilt angles to represent different orientations of the drone.

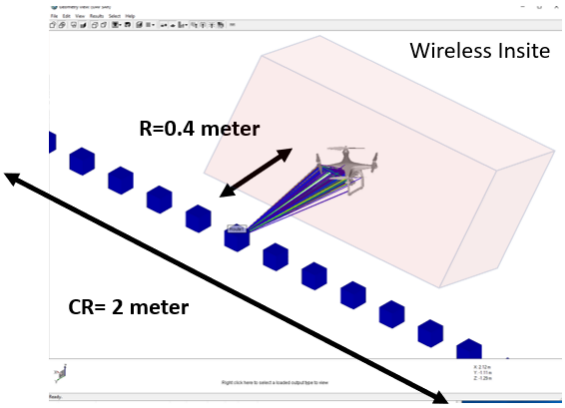

Fig. 2. SAR simulation model by Wireless Insite.

3. LABORATORY SAR IMAGES

3.1 EFFECT OF DRONE ORIENTATION AND CR

The effect of drone orientation is illustrated in Figs. 3~7 with a summary figure shown in Fig. 8. After exploring various parameters for the detection of drone orientation, we found that the ratio of integrated amplitude (I_{int}) to the maximum amplitude (I_{max}) decreases with respect to the drone orientation angle as it decreases from 90° to 0°. In other words, increasing the drone's orientation angle decreases I_{int}/I_{max}. Figs. 3-7 show the SAR images at CR = 0.4 m.

When we increased the CR from 0.4 m to 2.0 m, we found similar results, shown in Figs. 9-11. Increasing the CR from 0.4 m to 2.0 m increased the SAR amplitude, as shown in Figs. 9-11. With the improvement of cross-range resolution, the performance of SAR parameter I_{int}/I_{max} also appears to improve in Fig. 11. This indicates the potential of using SAR imaging for detecting drone orientation.

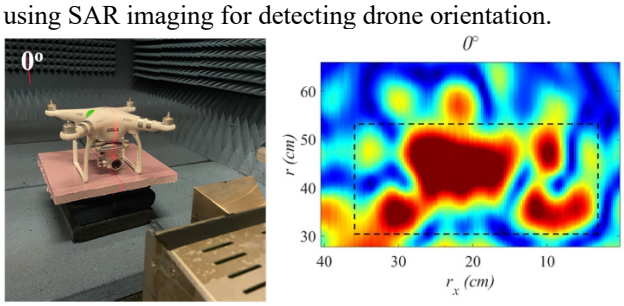

Fig. 3. SAR images of drone at 0°.

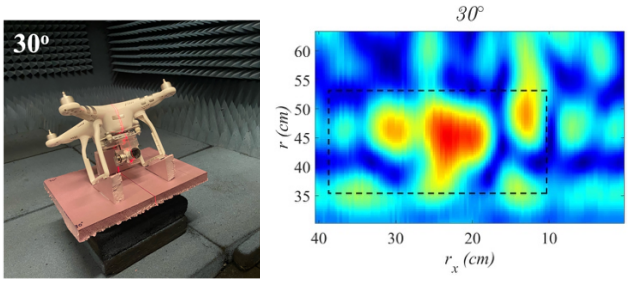

Fig. 4. SAR images of drone at 30°.

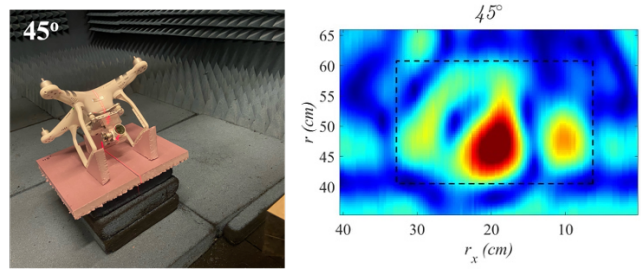

Fig. 5. SAR images of drone at 45°.

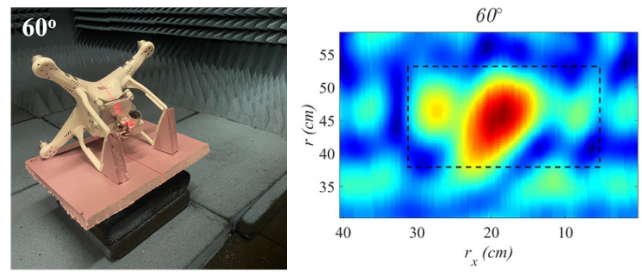

Fig. 6. SAR images of drone at 60°.

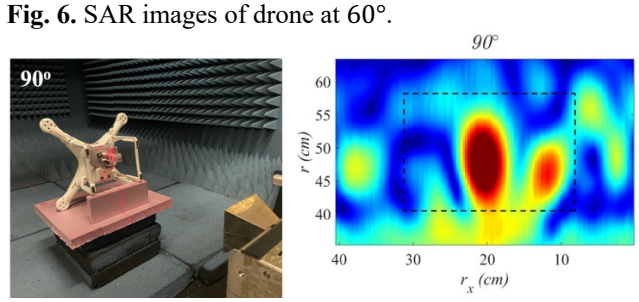

Fig. 7. SAR images of drone at 90° and summary.

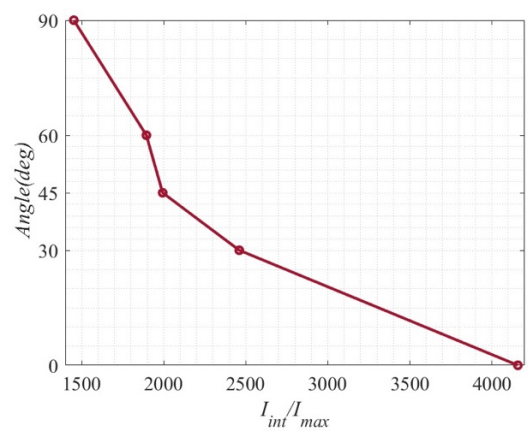

Fig. 8. Relation between drone orientation angle and I_{int}/I_{max} at R=0.4 m and CR=0.4 m.

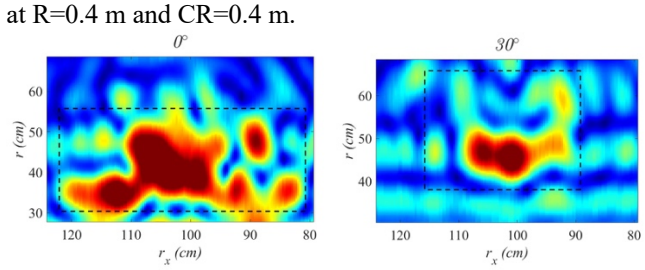

Fig. 9. SAR images of drone at 0° and 30°.

Authorized licensed use limited to: NIST Virtual Library (NVL). Downloaded on July 09,2025 at 17:37:20 UTC from IEEE Xplore. Restrictions apply.

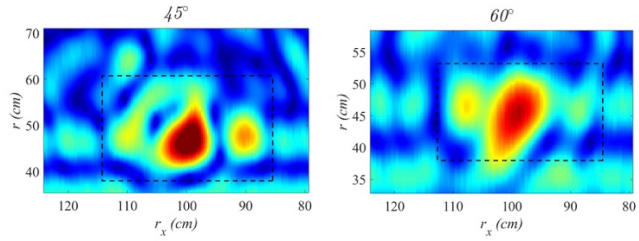

Fig. 10. SAR images of the drone at 45° and 60°.

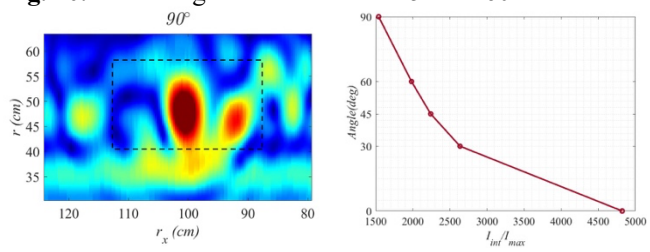

Fig. 11. SAR image of drone at 90° and relation of drone orientation angle to I_{int}/I_{max} at R = 0.4 m and CR = 2.0 m.

3.2 EFFECT OF RANGE

The SAR amplitude decreased as expected when we increased the range from 0.4 m to 1.0 m. Fig. 12 compares the SAR images of the drone at 45°. As expected, the SAR amplitude at R = 1.0 m overall decreased from R = 0.4 m. However, the scatterer representing the gimbal camera became weaker than other scatterers representing the drone's body. We show the performance of the SAR parameter I_{int}/I_{max} in Fig. 13. The one-to-one decreasing relationship of drone orientation angle to I_{int}/I_{max} is preserved.

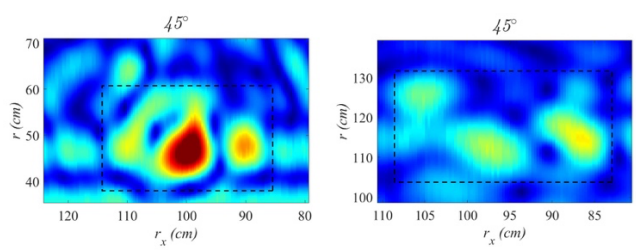

Fig. 12. SAR images of drone at R = 0.4 m and 1.0 m.

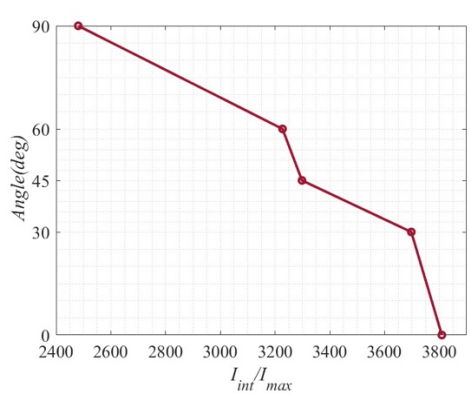

Fig. 13. Relation between drone orientation angle and I_{int}/I_{max}. at R = 1.0 m and CR = 2.0 m.

3.3 EFFECT OF BRICK WALL

Fig. 14 illustrates three imaging setups: (a) brick wall only, (b) brick wall with the drone at 0°, and (c) brick wall with the drone at 90°. From the result shown in Fig. 15~17 (R = 0.4 m, CR = 0.4 m), the SAR imaged the brick wall. We found that the drone in the SAR images blocked part of the brick wall. However, the SAR image of the drone remained detectable in these figures.

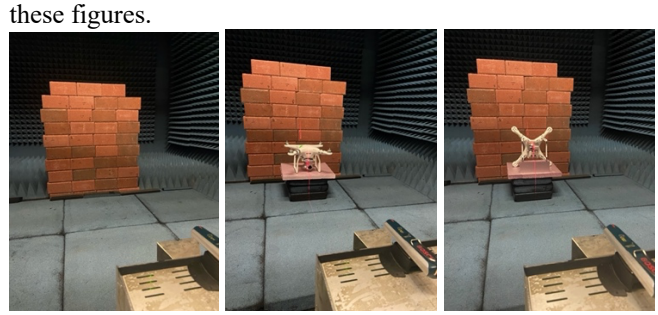

(a) Brick wall. (b) Brick wall with drone at 0°. (c) At 90°.

Fig. 14. Three SAR imaging setups.

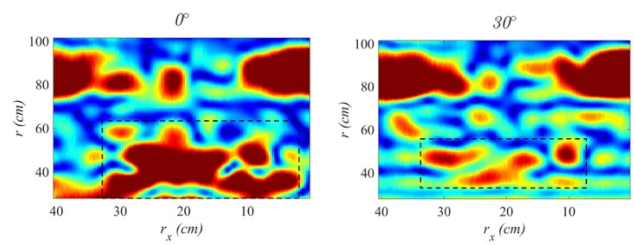

Fig. 15. 0° and 30° images with a brick wall.

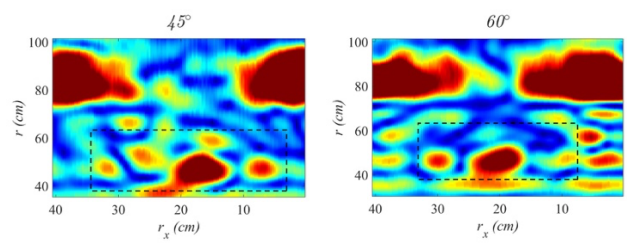

Fig. 16. 45° and 60° images with a brick wall.

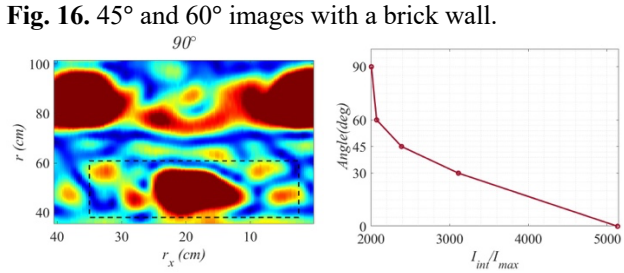

Fig. 17. 90° SAR images with brick wall and summary at R = 0.4 m and CR = 0.4 m.

Figs. 18-20 show the SAR images of the drone with a brick wall with R = 0.4 m and CR = 2.0 m. Comparing Figs. 18-20 (CR = 2.0 m) to Figs. 15-17 (CR = 0.4 m), we can see the improvement in the SAR image of the drone due to the improved cross-range resolution. Satisfactory performance of SAR image parameter I_{int}/I_{max} in both CR = 0.4 m and CR = 2.0 m is demonstrated in Figs. 17 and 20. Figs. 21-23

Authorized licensed use limited to: NIST Virtual Library (NVL). Downloaded on July 09,2025 at 17:37:20 UTC from IEEE Xplore. Restrictions apply.

show the SAR images of the drone with a brick wall with R = 1.0 m and CR = 0.4 m. We found similar results in Figs. 21-23. In general, the presence of a brick wall did not change the SAR image of the drone. But the relation between parameter I_{int}/I_{max} and the drone orientation angle was affected by the presence of a brick wall for all combinations (R, CR) of range and cross-range values, including (0.4, 0.4) m, (0.4, 2) m, (1, 0.4) m, and (1, 2) m.

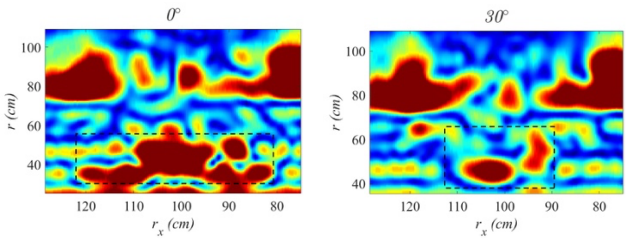

Fig. 18. 0° and 30° images with a brick wall.

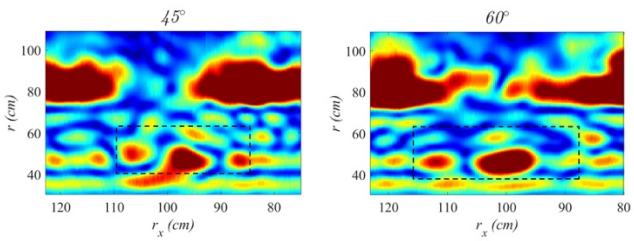

Fig. 19. 45° and 60° images with a brick wall.

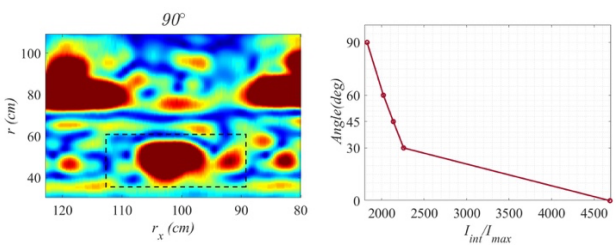

Fig. 20. 90° SAR images with brick wall and summary at R = 0.4 m and CR = 2.0 m.

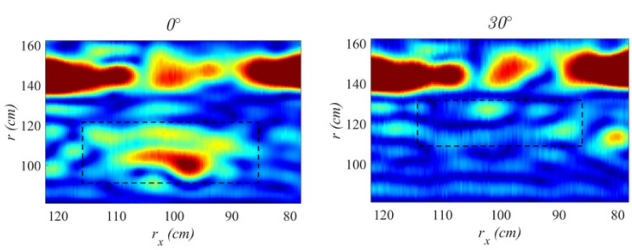

Fig. 21. 0° and 30° images with a brick wall.

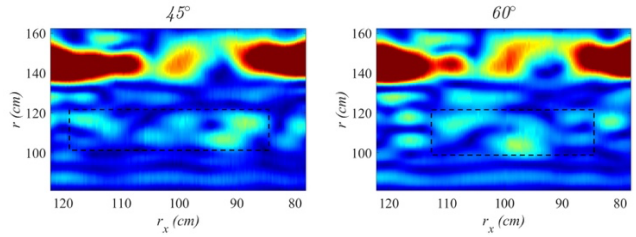

Fig. 22. 45° and 60° images with a brick wall.

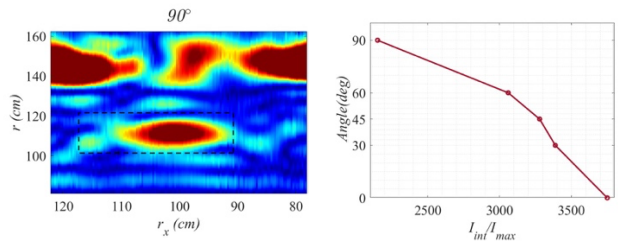

Fig. 23. 90° SAR images with brick wall and summary at R = 1.0 m and CR = 0.4 m.

4. SIMULATED SAR IMAGES

To generate SAR images from the simulated model, we projected the MPCs (Multipath Components) generated by the CAD model from spherical to cartesian coordinates. The projected scatter centers that fall into the same range cell and angle resolution bin were combined into a single scatter center based on the maximum power. The final scatter centers feed into the SAR image algorithm is shown in Fig. 24. The maximum received linear power was normalized to unity.

A spotlight SAR imaging algorithm was used to generate the SAR image shown in Fig. 25 [5, 6]. The parameters of the FMCW used for simulation matched those used in the laboratory experiment. The edge of Fig. 3 was extracted with orange color and overlapped with the simulated SAR image. We found that the simulated image and the measured image exhibit correlated shapes. Comparing with heatmap between Fig. 3 and Fig. 25, we found that the relative power between scatter centers has a mismatch between the measured image and the simulated image because the software cannot configure material properties separately for each face. In the simulation, it was assumed that the entire UAV is plastic, while the real UAV contains metal parts.

Authorized licensed use limited to: NIST Virtual Library (NVL). Downloaded on July 09,2025 at 17:37:20 UTC from IEEE Xplore. Restrictions apply.

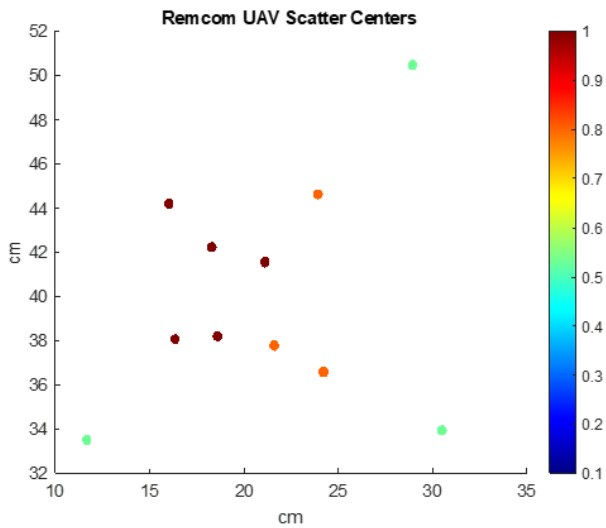

Fig. 24. UAV scatter centers generated by Wireless Insite at 0 degrees tilt.

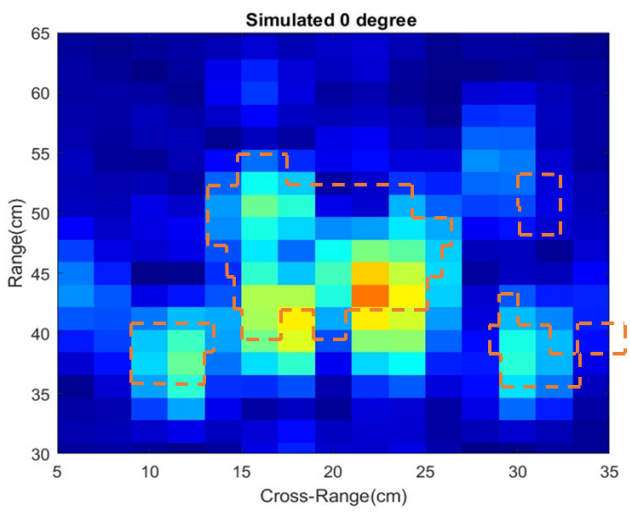

Fig. 25. Simulated SAR image at 0° orientation.

5. SUMMARY

In summary, we presented our physically measured images and numerically simulated SAR images of a drone target with a laboratory 10 GHz FMCW SAR imaging system. We found that the variation in the drone orientation angle in the range of 0° and 90° (0°, 30°, 45°, 60°, and 90°) can be detected by our laboratory SAR imaging system at two different ranges (R=0.4 m and 1 m) and two different cross-ranges (CR=0.4 m and 2 m). The ratio of the integrated SAR amplitude (I_{int}) to the maximum SAR amplitude (I_{max}) was found to show a decreasing pattern with the increase of the drone orientation angle from 0° and 90°. In general, the presence of a brick wall did not change the SAR image of the drone. But the relation between parameter I_{int}/I_{max} and the drone orientation angle was affected by the presence of a brick wall for all combinations (R, CR) of range and cross-range values, including (0.4, 0.4) m, (0.4, 2) m, (1, 0.4) m, and (1, 2) m. Our numerical simulation also showed that the simulated SAR image and the measured SAR image are qualitatively correlated with a quantitative difference due to the discrepancy in material properties.

6. ACKNOWLEDGEMENT

The authors (Abazarsa and Yu) would like to thank graduate students Shrilekha Medarapu and Shwe Wah San for their assistance in laboratory experimentation.

7. REFERENCES

[1] D.R. Reagan, C. Niezrecki, T. Yu, A. Sabato, R. Wilson, "An autonomous unmanned aerial vehicle sensing system for structural health monitoring of bridges," *Proc SPIE Smart Structures/NDE*, Mar. 20-24, Las Vegas, NV, 2016.

[2] N. Bashir, S. Boudjit, S. Zeadally, "A closed-loop control architecture of UAV and WSN for traffic surveillance on highways," *Computer Communications* 190; 78-86, 2022.

[3] J. Struaub, "Unmanned aerial systems: Consideration of the use of force for law enforcement applications," *Technology in Society* 39; 100-109, 2014.

[4] I. You, M.R. Ogiela, A.M. Tjoa, D. Shin, "Advanced technologies for homeland defense and security," *Journal of Network and Computer Applications* 38; 1-2, 2014.

[5] W. G. Carrara, R. S. Goodman, and R. M. Majewski, *Spotlight Synthetic Aperture Radar: Signal Processing Algorithms*, Artech House, 1995.

[6] Mehrdad Soumekh, *Synthetic Aperture Radar Signal Processing with MALAB Algorithms*, Wiley, 1999.

Authorized licensed use limited to: NIST Virtual Library (NVL). Downloaded on July 09,2025 at 17:37:20 UTC from IEEE Xplore. Restrictions apply.